Release Currents of IP_3 Receptor Channel Clusters and Concentration Profiles

R. Thul and M. Falcke
Hahn Meitner Institut, 14109 Berlin, Germany

ABSTRACT We simulate currents and concentration profiles generated by Ca^{2+} release from the endoplasmic reticulum (ER) to the cytosol through IP_3 receptor channel clusters. Clusters are described as conducting pores in the lumenal membrane with a diameter from 6 nm to 36 nm. The endoplasmic reticulum is modeled as a disc with a radius of 1–12 μm and an inner height of 28 nm. We adapt the dependence of the currents on the *trans* Ca^{2+} concentration (intralumenal) measured in lipid bilayer experiments to the cellular geometry. Simulated currents are compared with signal mass measurements in *Xenopus* oocytes. We find that release currents depend linearly on the concentration of free Ca^{2+} in the lumen. The release current is approximately proportional to the square root of the number of open channels in a cluster. Cytosolic concentrations at the location of the cluster range from 25 μM to 170 μM. Concentration increase due to puffs in a distance of a few micrometers from the puff site is found to be in the nanomolar range. Release currents decay biexponentially with timescales of $<$1 s and a few seconds. Concentration profiles decay with timescales of 0.125–0.250 s upon termination of release.

INTRODUCTION

Many cells control the cytosolic Ca^{2+} concentration by release and uptake of Ca^{2+} from intracellular stores like the endo- and sarcoplasmic reticulum. Ca^{2+} flows down its electrochemical gradient upon opening of channels on the membrane of these stores. One of these channels is the inositol 1,4,5-trisphosphate receptor channel (IP_3R), which is found in many different cells (Berridge, 1993, 1997; Berridge et al., 1998). Because the opening probability of the IP_3R depends on the cytosolic Ca^{2+} concentration, channels can communicate with each other via the released Ca^{2+}. Thus complex spatiotemporal patterns are formed. (Ridgway et al., 1977; Lechleiter et al., 1991; Nathanson et al., 1994; D'Andrea and Vittur, 1995; Marchant et al., 1999; Marchant and Parker, 2001; Bootman et al., 1997, 2001). This extensive behavior of intracellular Ca^{2+} dynamics has caused a great amount of modeling studies (Dupont and Goldbeter, 1993, 1994; Borghans et al., 1997; DeYoung and Keizer, 1992; Wagner and Keizer, 1994; Atri et al., 1993, Sneyd et al., 1993; Sneyd and Sherrat, 1997; Sneyd and Dufour, 2002; Falcke et al., 1999a,b, 2000a; Bär et al., 2000; Falcke, 2003a,b).

However, despite the fact that release through a single IP_3 receptor channel or a closely packed group of channels is in the core of the dynamics, it has attracted less attention. Although several studies on the concentration dynamics close to open ryanodine receptor channels exist, little has been done for the IP_3R (Melzer et al., 1984, 1987; Blatter et al., 1997; Smith et al., 1998; Izu et al., 2001; Pratusevitch and Balke, 1996; Mejia-Alvarez et al., 1999; Rios et al., 1999; Gonzalez et al., 2000) but see Swillens et al. (1998) for IP_3R. The major differences between release through ryanodine receptor channels and IP_3Rs are the currents and timescales. Currents between 0.35 and 3.3 pA are observed in experiments mimicking release from the sarcoplasmic reticulum and elemental events last typically ~10 ms (Rios et al., 1999; Mejia-Alvarez et al., 1999). Currents through a single IP_3R are estimated to be in the range from 0.1 to 0.5 pA and elemental events last a few hundred milliseconds (Parker et al., 1996a; Sun et al., 1998). Hence, peak concentrations, the spread of free Ca^{2+} in the cytosol and the development of the store content will be different from release by ryanodine receptor channels.

The existing simulations and analytic calculations demonstrate that huge concentration gradients occur around release sites (Smith et al., 2001). Furthermore, the arrangement of channels in small groups or as single channels on the ER membrane creates spatially discrete release sites (Sun et al., 1998; Marchant and Parker, 2001; Mak et al., 2000; Mak and Foskett 1997, 1998; Wilson et al., 1998). The typical distance between these release sites is a few micrometers (Marchant and Parker, 2001; Thomas et al., 1998) and therefore larger than the diffusion length of free Ca^{2+} in the cytosol of 0.4–1.3 μm (Wang and Thompson, 1995). Hence, concentration values can differ by 2–3 orders of magnitude between the locations of neighboring channels or channel clusters. Several theoretical studies have shown that the consequences of the discreteness and the concentration gradients can reach from the loss of the ability to oscillate (Sneyd and Sherrat, 1997; Falcke, 2003b) to the termination of wave propagation (Sneyd and Sherrat, 1997; Falcke et al., 2000b; Coombes, 2001). It is therefore important to know at least approximately the concentration values, gradients, and dynamics at the mouth of a releasing channel and at a distance of a few micrometers. The purpose of this study is to provide a quantitative idea of these release characteristics to support further modeling of intracellular Ca^{2+} dynamics. That goal is different from other studies aiming at the interpretation and evaluation of specific experiments, e.g., by drawing conclusions from dye concentration profiles with

Submitted July 8, 2003, and accepted for publication December 9, 2003.
Address reprint requests to M. Falcke, E-mail: falcke@hmi.de.

0006-3495/04/05/2660/14 $2.00

respect to the profile of free Ca^{2+} (Melzer et al., 1984, 1987; Blatter et al., 1997; Smith et al., 1998; Pratusevitch and Balke, 1996; Mejia-Alvarez et al., 1999; Rios et al., 1999; Gonzalez et al., 2000). The study at hand contains much information that is experimentally relevant as well, especially because we tried to model as close to experimental findings as possible.

We will consider the process of Ca^{2+} release through an open channel. The dynamics of the channel state (open, closed, or inhibited) is not the subject of this study. Because the channel current through the IP_3R in vivo is not very well known, we will start from lipid bilayer experiments. We will transfer their results on the dependence of channel currents on lumenal concentrations to in vivo geometries and concentrations. The following section introduces the model equations and explains the choice of parameter values. The subsequent section will present simulation results. We find that the release currents depend linearly on the concentration of free Ca^{2+} in the lumen but are less sensitive to lumenal buffer concentrations, total lumenal Ca^{2+} content, or lumenal diffusion coefficients for ranges of values that can be expected to hold in vivo. The release current is approximately proportional to the square root of the number of open channels in a cluster. Cytosolic concentrations at the location of the cluster range from 25 μM to 170 μM. Concentration increase due to open clusters in a distance of a few micrometers is found to be in the nanomolar range on the timescale of puff duration. Concentration profiles built up by release decay on a timescale of 0.125–0.250 s. Release currents decay biexponentially with timescales of <1 s and a few seconds.

METHODS AND PARAMETERS

We simulate release of Ca^{2+} in a cylindrical volume divided by the lumenal membrane perpendicular to the cylinder axis. The smaller part represents the ER and the larger part the cytosol. The channel is a pore in the center of the ER membrane with radius R_s (see Fig. 1). The initial condition is the stationary Ca^{2+} distribution resulting from the pumps and the leak flux P_l. No flux boundary conditions were applied at the outer surface of the cylinder. We chose cylindrical coordinates for our simulations with the positive z-direction pointing from top to bottom in Fig. 1.

The model comprises the following species:

The cytosolic free Ca^{2+} concentration c.
The free Ca^{2+} concentration in the endoplasmic reticulum E.
The concentration of stationary buffer b_s in the cytosol with Ca^{2+} bound.
The concentration of mobile buffer b_m in the cytosol with Ca^{2+} bound.
The concentration of stationary buffer b_{Es} in the endoplasmic reticulum with Ca^{2+} bound.
The concentration of mobile buffer b_{Em} in the endoplasmic reticulum with Ca^{2+} bound.

The reaction-diffusion equations in the cytosol are:

$$\frac{\partial c}{\partial t} = D\nabla^2 c - k_m^+ (B_m - b_m)c + k_m^- b_m - k_s^+ (B_s - b_s)c + k_s^- b_s$$

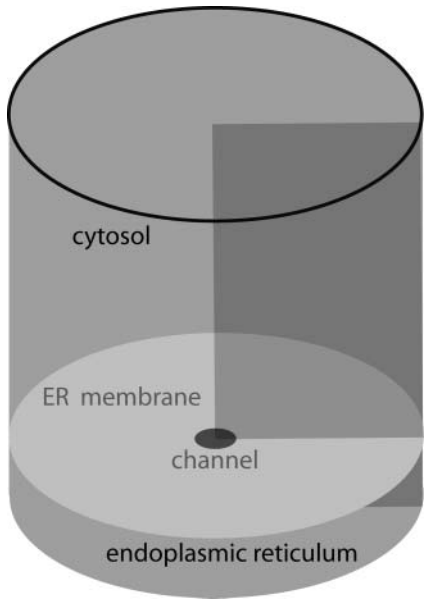

FIGURE 1 Volume within which release was simulated. Rotational symmetry allows us to reduce the integration to a plane cutting radially into the volume as shown.

$$\frac{\partial b_m}{\partial t} = D_m\nabla^2 b_m + k_m^+ (B_m - b_m)c - k_m^- b_m$$

$$\frac{\partial b_s}{\partial t} = k_s^+ (B_s - b_s)c - k_s^- b_s.$$

The equations include diffusion of free Ca^{2+} c ($D\nabla^2 c$), diffusion of mobile buffer b_m ($D_m\nabla^2 b_m$), and the reactions of stationary buffer b_s and mobile buffer b_m with free Ca^{2+} ($k_i^+ (B_i - b_i)c - k_i^- b_i$, B_i total buffer concentration, $i = s,m$).

Analogously, the dynamics in the endoplasmic reticulum are:

$$\frac{\partial E}{\partial t} = D_E\nabla^2 E - k_{Em}^+ (B_{Em} - b_{Em})E + k_{Em}^- b_{Em} - k_{Es}^+ (B_{Es} - b_{Es})E + k_{Es}^- b_{Es}$$

$$\frac{\partial b_{Em}}{\partial t} = D_{Em}\nabla^2 b_{Em} + k_{Em}^+ (B_{Em} - b_{Em})E - k_{Em}^- b_{Em}$$

$$\frac{\partial b_{Es}}{\partial t} = k_{Es}^+ (B_{Es} - b_{Es})E - k_{Es}^- b_{Es}.$$

The flux J through the membrane separating ER and cytosol is given by:

$$J = \Psi \frac{E - \alpha c}{\beta + \gamma E + \delta c}, \quad r \le R \tag{1}$$

$$J = P_l(E - c) - P_p \frac{c^2}{K_d^2 + c^2}, \quad r > R. \tag{2}$$

Here, the values of E and c have to be taken at the membrane (position z_m). R denotes the cluster radius, P_l the coefficient of the leak flux density, and P_P the maximal pump strength. The constants in Eq. 1 will be

determined in the next section. The currents are incorporated into the volume dynamics by setting the boundary condition at the ER membrane like:

$$D\frac{\partial c}{\partial z} = D_{\mathrm{E}}\frac{\partial E}{\partial z} = J. \tag{3}$$

Fitting the single channel flux

The expression for the flux through an open channel (Eq. 1) is fitted to data by Bezprozvanny and Ehrlich (1994). Bezprozvanny and Ehrlich measured single channel currents of channels reconstituted into planar lipid bilayers with Ba^{2+} as charge carrier in dependence on the *trans* (lumenal) concentration. The constants of Eq. 1 are fitted by simulation of fluxes in these experiments. To perform a fit to the data, we need to mimic the spatial set up of the diffusion problem for a single channel. The current through a single channel is determined, among other parameters, by the geometry of the channel pore. The size of the channel pore is in the range from 10 $Å^2$ (Hille, 2001) to 40 $Å^2$ (Lindsay and Williams, 1991; Lindsay et al., 1991), if we assume it to be similar to the pore of the ryanodine receptor channel. However, we are interested in concentration profiles on the length scale of a few micrometers. We need to find a compromise in terms of length scales between the geometry of the channel pore and the micrometer length scale to reach a computationally treatable model. Here, we use results of Mejía-Alvarez et al. (1999) who performed similar simulations for ryanodine receptor channels. They estimated the size of the channel sponge on the lumenal side of the ryanodine receptor channel. The channel sponge is the volume within which negative charges surrounding the channel pore reside. The radius of this sponge was calculated to be the radius of the Donnan equilibrium potential created by the negative charges (Mejia-Alvarez et al., 1999). It was estimated to be ~5–10 nm (Mejia-Alvarez et al., 1999). Therefore, we consider the channel to be a conducting pore in the membrane of approximately this radius. In most simulations we use 6 nm (allowing for a numerical grid mesh size of 2 nm).

The *trans* chamber in the simulations used to fit the dependence of the current on lumenal concentrations has a radius of 12 μm and a thickness of 6.24 μm. The *cis* chamber is set up with the same radius and is 5.22 μm thick. These measures are sufficient to exclude geometric restrictions, i.e., could serve as a model of a chamber much larger than $(12\ \mu\mathrm{m})^2\pi \times 5.22\ \mu$m. The diffusion coefficient for free Ca^{2+} is set to 600 $\mu m^2\ s^{-1}$ corresponding to the value in water (Kushmerick and Podolsky, 1969). The *cis* chamber contains 4 mM of mobile buffer ($k_m^+ = 404.67\ (\mu\mathrm{Ms})^{-1}$, $k_m^- = 100\ s^{-1}$, $D_m = 30\ \mu m^2\ s^{-1}$) and 100 μM of stationary buffer ($k_s^+ = 50\ (\mu\mathrm{Ms})^{-1}$, $k_s^- = 100\ s^{-1}$). However, the buffers have essentially no effect on the current values.

As suggested by the data of Bezprozvanny and Ehrlich (1994), we take a saturating barrier model of a conducting pore with one ion binding site for the flux (Keener and Sneyd, 1998). The general expression of the flux through such a pore is given by Eq. 1. Note, that only four of the five constants in this equation are independent. To fit them to the data by Bezprozvanny and Ehrlich we simulate the current I in bilayer experiments. The current is equal to the integral of the flux density over the pore cross section $I = 2F\int_0^{R_s} 2\pi r J\, dr$ (F Faraday's constant, r radial coordinate, z_m axial coordinate of the membrane, R_s single channel radius). We performed simulations for the homogeneous initial values $E = 10, 20, 30, 40$ mM, which were also used in the experiments. In these simulations for the fitting procedure, the expression $J = P_{ch}(E - c)$ was used for the channel flux density. Adjusting P_{ch} for each of the four lumenal Ca^{2+} concentrations in such a way as to reproduce the measured currents allows us to read off the values of the lumenal and cytosolic free Ca^{2+} concentration at the channel and to determine the constants in Eq. 1: $\Psi = 9.3954\ \mu\mathrm{ms}^{-1}$, $\alpha = 1.1497$, $\beta = 1.1949\ 10^{-3}$, $\gamma = 1.1444\ 10^{-7}\ \mu\mathrm{M}^{-1}$, and $\delta = 1.1556\ 10^{-7}\ \mu\mathrm{M}^{-1}$.

Local depletion of Ca^{2+} due to the channel flux does not occur in this geometry and with these concentration values and diffusion coefficients. That can be concluded from the values of E at the channel $E = 9.5, 19.3, 29.2,$ and 39.2 mM belonging to the initial concentrations 10, 20, 30, 40 mM. Hence, the concentration at the channel is well approximated by concentration values in the bulk of the chamber far away from the channel in lipid bilayer experiments. We will see below that this does not apply to in vivo situations. The results for the constants of Eq. 1 imply a half maximum value (β/γ) of 10.44 mM for E, which is close to the value of 9 mM given in Bezprozvanny and Ehrlich (1994). The difference $E - \alpha c$ remained large in this lipid bilayer simulation. Hence, there is little effect of Ca^{2+} on the *cis* (cytosolic) side on channel flux density in the lipid bilayer experiments. We will see below, that the concentration values on the lumenal and cytosolic side can be close to each other and the feedback by cytosolic Ca^{2+} becomes relevant in different geometries and for different concentrations in the lumenal part.

Other parameter values

According to Alberts et al. (1994; p. 580), the lumenal space of a flattened cistern of the endoplasmic reticulum of a liver cell is 20–30-nm wide. The diameter of tubes belonging to the network part of the ER is up to 60 nm. We will consider the case of release from cisternae with a thickness of 28 nm and tubular networks. Tubular networks are not described by implementing their real geometry in the simulations. We still use the same cylindrical geometry. However, diffusional transport is reduced due to the tubular shape of the network compared to unobstructed volume and we have to incorporate this reduction. Here, we take advantage of results by Ölveczky and Verkman, who showed that the turtuosity of such a tubular network can be accounted for by reducing the diffusion coefficient by 40–60% (Ölveczky and Verkman, 1998). Hence, we model tubular networks by a disc with a height of 60 nm and a reduction of lumenal diffusion coefficients to one-half of the values for cisternae.

The endogenous cytosolic buffer capacity (B_s/K_s) of immobile buffer was chosen to be ~40 according to findings by Zhou and Neher (1993). In agreement with the same experiments, that buffer has a rather large dissociation constant of 2 μM.

The diffusion coefficient of free Ca^{2+} in the cytosol was measured by Allbritton et al. as 223 $\mu m^2\ s^{-1}$ (Allbritton et al., 1992). The diffusion coefficient of Ca^{2+} in water is ~600 $\mu m^2\ s^{-1}$ (Kushmerick and Podolsky, 1969). It was found, that the diffusion coefficients of substances in the cytosol, which are believed not to be bound in the cytosol, are approximately one-half of the value in water (Kushmerick and Podolsky, 1969). This observation supports the value measured by Allbritton et al. (1992) and hence we adopt that value as the diffusion coefficient of free Ca^{2+} in the cytosol. It is difficult to estimate the diffusion coefficient of free Ca^{2+} in the ER. In most of the simulations, we use the same value as in the cytosol. However, one could assume that similar to the reduction of diffusion when going from water to the cytosol by one-half, a further reduction occurs when going from the cytosol to the lumen of the endoplasmic reticulum. Hence, we will show results with diffusion coefficients of free Ca^{2+} in the ER reduced by one-half with respect to value in the cytosol, too.

The results of the measurements of the total Ca^{2+} content of the ER depend on the method used. Direct determination by electron microscopy techniques finds a range of 5–50 mM. The highest values occur in the terminal cisternae of the sarcoplasmic reticulum (Meldolesi and Pozzan, 1998). Indirect measurements based on fluorescent indicators in the cytosol find 5–10 mM (Meldolesi and Pozzan, 1998).

Most of the lumenal Ca^{2+} is bound to buffer. The buffer protein calsequestrin is predominantly found in muscle cells. It binds Ca^{2+} with high capacity (≈50 ions per molecule) and a K_d of 1 mM (Meldolesi and Pozzan, 1998). Calreticulin is mostly found in nonmuscle cells. It binds 20–50 Ca^{2+} ions with low affinity ($K_d = 0.3$–2.0 mM) (Michalak et al., 1992). Changing the lumenal concentration of calreticulin has complex consequences for IP_3-induced Ca^{2+} release (Camacho and Lechleiter, 1995; Roderick et al., 1998; John et al., 1998).

The concentration of free Ca^{2+} in the endoplasmic reticulum is especially important because it is the driving force for release. It is typically in the range of a few hundred μM and may reach up to 1 mM (Meldolesi and

Pozzan, 1998). A few examples of specific measurements are: in rat embryo R6 fibroblasts 500 μM (Foyouzi-Youssefi et al., 2000), in rat myotubes sarcoplasmic reticulum after 6 days in culture 300 μM (Robert et al., 1998), in BHK21 fibroblasts 539 $\pm$ 92 μM (Hofer and Schulz, 1996), in HeLa cells 60–400 μM (Miyawaki et al., 1997). More values can be found in Meldolesi and Pozzan (1998).

We translate these findings into parameter values for buffers in the endoplasmic reticulum. We use the total concentration of buffers to control the total Ca^{2+} content of the ER and the buffer dissociation constant to set the concentration of free Ca^{2+}. We will show examples with a total content in the range from 5.24 mM to 67.87 mM and a free concentration from 127 μM to 715 μM. Similarly, diffusion coefficients of mobile buffers in the lumen of the ER could only be guessed. Consequently, we vary this parameter from 0 to 30 $\mu m^2\ s^{-1}$.

Numerical simulations use a 4th order Runge Kutta algorithm (Press et al., 1992). Spatial discretization was 2 nm for single channel simulations, $2\sqrt{2}$ nm and 4 nm for larger clusters. The time discretization is chosen between 25% and 90% of the stability criteria (Press et al., 1992).

RESULTS

All results presented in this section are obtained in the cell-like geometry. Thus, the lumenal height is set to 28 nm when we refer to cisternae in the ER and 60 nm for the tubular ER. Additionally we reduce the diffusion coefficient in the latter case. We begin the presentation with simulation results for single channels. The concentration in a vicinity of a few nanometers of the channel mouth rises within microseconds upon opening of a channel. On the same timescale of microseconds, the concentration of free lumenal Ca^{2+} at the channel vestibule drops to create the large gradients necessary to transport Ca^{2+} to the channel. All ensuing slow relaxations cause concentration changes typically an order of magnitude smaller than this initial fast rise. This very fast initial timescale appears in the current as well. It quickly drops within the first microseconds to a level that then changes on the timescale of milliseconds.

A channel opens and closes rapidly once it is activated. Typical dwell times are in the range of a few milliseconds (see, e.g., Mak and Foskett, 1998; Mak et al., 2001)). The concentrations of fast buffers and free Ca^{2+} within a vicinity of <1 μm follow or are influenced by this rapid opening and closing of the channel. That is demonstrated in Fig. 2. The concentrations immediately at the channel react with a sharp rise or drop upon channel opening and closing.

Upon closing of the channel, cytosolic free Ca^{2+} drops from $\sim$74 μM to 93 nM within 1 ms and to 65 nM within the next 4 ms (see Fig. 2). These latter values are a factor 3–4 larger than the resting level but negligible compared to the concentration value for an open channel. The cytosolic mobile buffer with Ca^{2+} bound has a resting value of 2.9 μM and drops to 3.89 μM in between current pulses. The concentration changes of free cytosolic Ca^{2+} due to the rapid opening and closing of the channel are already considerably damped at a distance of 1 μm from the channel. In a range of 2 μm from the channel, Ca^{2+} rises monotonically (Fig. 2). Note that the Ca^{2+} concentrations in the cytosol in Fig. 2 and in all following figures are presented as the increase above resting

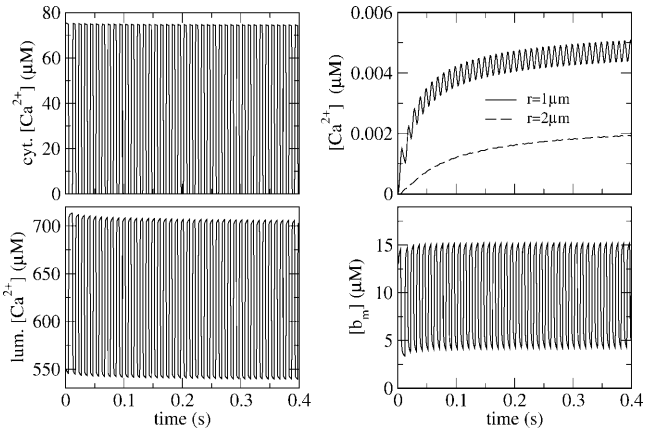

FIGURE 2 Concentration values of cytosolic free Ca^{2+} at the channel mouth (*top left*) and in a distance of 1 μm and 2 μm (*top right*), lumenal free Ca^{2+} at the channel vestibule (*bottom left*), and cytosolic mobile buffer with Ca^{2+} bound at the channel mouth (*bottom right*). Open and closed times are 5 ms each. For parameter values, see Set 2 in Table 1. The amplitude of the current pulses is $\sim$0.0785 pA and decreases by 1% only in the first 400 ms (data not shown).

level. The dynamics of slow buffer shows a smaller amplitude than the fast buffer fluctuations. If we reduce k_m^- from 170 s^{-1} to 20 s^{-1} while keeping the value of the dissociation constant K_m, the amplitude of fluctuations of mobile Ca^{2+}-bound buffer drops from 11.45 μM to 2.73 μM.

When more than one channel in a cluster is activated, the channels open and close on a timescale of a few milliseconds. This leads to an average number of permanently open channels. Therefore we simulate clusters with a given number N_O of open channels. Channels in a cluster are assumed to be closely packed with a distance of 12 nm (Swillens et al., 1999). Release through the different channels of a cluster cannot be considered as independent, if the width of the concentration profile formed in the lumen equals approximately or is larger than channel spacing. Our simulations showed that a single channel release current of 0.041 pA causes a profile of free Ca^{2+} in the lumen with a full width at half-depth of 10 nm after 15 ms. Hence, the total release current of a cluster is not the sum of the single channel currents but channels influence each other. That interaction of release through the different channels of a cluster is the reason for the relation between the number of open channels and current we will demonstrate below. Swillens and Dupont found that release through several closely packed individual channels can be very well approximated by release through a single membrane area of corresponding size (Swillens et al., 1999). Based on these observations we model a cluster with several open channels by setting the area of the conducting pore proportional to $N_O R_s^2$ with R_s being the single channel radius. The radius of the pore is then called cluster radius R and is determined by $R = \sqrt{N_O} R_s$. We will simulate release for the typical duration of a puff of 400 ms in most of the examples. The

TABLE 1 Parameters of simulations

Parameter	Set 1 Value	Set 2 Value	Unit
Geometric parameters			
Height of the cytosol	9	–	μm
Radius of the cytosol	12	–	μm
Height of the ER h_{ER}	0.028	0.060	μm
Radius of the ER R_{ER}	12	–	μm
Leak flux coefficient P_l	0.02	–	μm s^{-1}
Channel flux constants			
Ψ	9.3954	–	μm s^{-1}
α	1.497	–	
β	1.1949 10^{-4}	–	
γ	1.1444 10^{-7}	–	μM^{-1}
δ	1.1556 10^{-7}	–	μM^{-1}
Single channel radius R_s	0.006	–	μm
Pump flux coefficient P_p	40	–	μM μm s^{-1}
Pump dissociation constant K_d	0.2	–	μM
Diffusion coefficient			
D	223	–	μm^2 s^{-1}
D_E	223	110	μm^2 s^{-1}
D_m	40	–	μm^2 s^{-1}
D_{Em}	30	16.95	μm^2 s^{-1}
On-rates of buffers			
k_s^+	50	–	(μMs)$^{-1}$
k_m^+	700	–	(μMs)$^{-1}$
k_{Em}^+	1	–	(μMs)$^{-1}$
k_{Es}^+	1	–	(μMs)$^{-1}$
Buffer dissociation constants k_i^-/k_i^+:			
K_s	2	–	μM
K_m	0.2428	–	μM
K_{Es}	350	–	μM
K_{Em}	350	–	μM
Total concentrations of buffers			
B_s	80	–	μM
B_m	40	–	μM
B_{Es}	50	5	mM
B_{Em}	50	5	mM
Total concentration of Ca^{2+} in the ER	67.87	7.430	mM
Resting concentration of free Ca^{2+} in the ER	715.56	715.56	μM

Voids in the Set 2 value column mean that the value of Set 1 is valid.

section entitled "Long timescales, higher cluster density" will consider longer simulations.

The currents resulting from different numbers of open channels in a cluster for a high filling state of the ER are shown in Fig. 3. They remain essentially constant after an initial relaxation on timescales from a few milliseconds to a few tens of milliseconds for all numbers of open channels. The current increases by about a factor of 10 while going from 1 to 21.77 open channels.

The initial current going through the cluster immediately upon opening is a quadratic function of the cluster radius R. Because spatial profiles of the concentrations have not built up yet, it is proportional to the cluster area. The quadratic dependence quickly turns into an almost linear relationship $I = A_0 + A_1R$ as the concentration profiles form. This linear approximation is valid for a certain range of radii only; e.g., it will not hold for $R \rightarrow 0$ because of the constant term A_0. However, it is surprisingly good for radii between 6 nm and 50 nm. Therefore, currents are proportional to the square root of the number of open channels in that range. The increase of the current with the cluster radius is sublinear for low Ca^{2+} content of the ER (see Fig. 4).

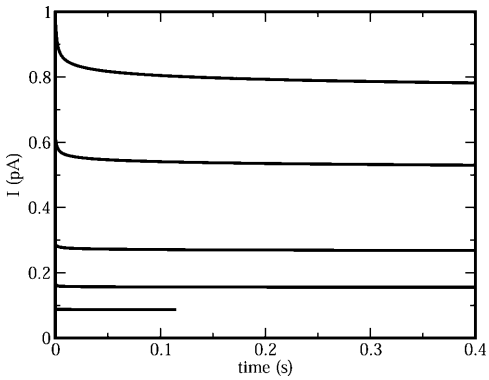

FIGURE 3 Dependence of currents on time. The lines show results for 1, 2, 4, 11.11, and 21.77 open channels from lower to higher values. For parameter values, see Set 1 in Table 1. Release through a single channel was simulated for 0.115 s only.

Concentration values at different distances from the cluster are shown in Fig. 5. Note, that an increase in the number of open channels from 1 to 21.77 entails a rise of the concentration of free cytosolic Ca^{2+} at the location of the cluster from ~100 μM to ~170 μM only. Hence, the number of open channels and the currents are not very well reflected by the peak concentration values of cytosolic Ca^{2+} (see as well Fig. 7, 8, 10). This is different for concentrations

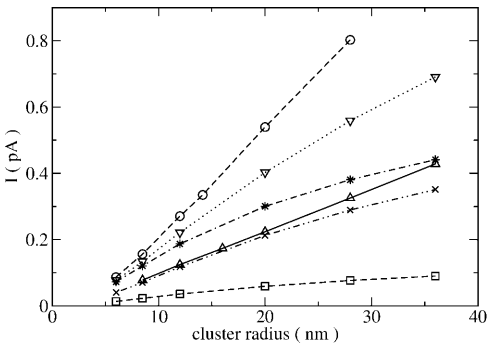

FIGURE 4 Dependence of current on cluster radius at $t = 0.1$ s. ($\triangle$) Set 1 except $h_{ER} = 0.06$ μm, $D_E = 23$ μm^2 s^{-1}, $D_{Em} = 3.1$ μm^2 s^{-1}. ($\bigcirc$) Set 1, except $B_{Es} = 100$ mM, $B_{Em} = 0$, (X) Set 1 except $E = 336$ μM, total lumenal content 5.24 mM, $B_{Es} = 100$ mM, $B_{Em} = 0$. (∇) Set 1 except total lumenal content 7.43 mM, $h_{ER} = 0.06$ μm, $D_E = 110$ μm^2 s^{-1}, $D_{Em} = 16.95$ μm^2 s^{-1}, $B_{Es} = 100$ mM, $B_{Em} = 0$. ($\square$) Set 1 except $E = 127.8$ μM, total lumenal content 2.80 mM, $B_{Es} = 100$ mM, $B_{Em} = 0$. (*) Set 1 except $E = 715$ μM, total lumenal content 7.43 mM, $B_{Es} = 100$ mM, $B_{Em} = 0$.

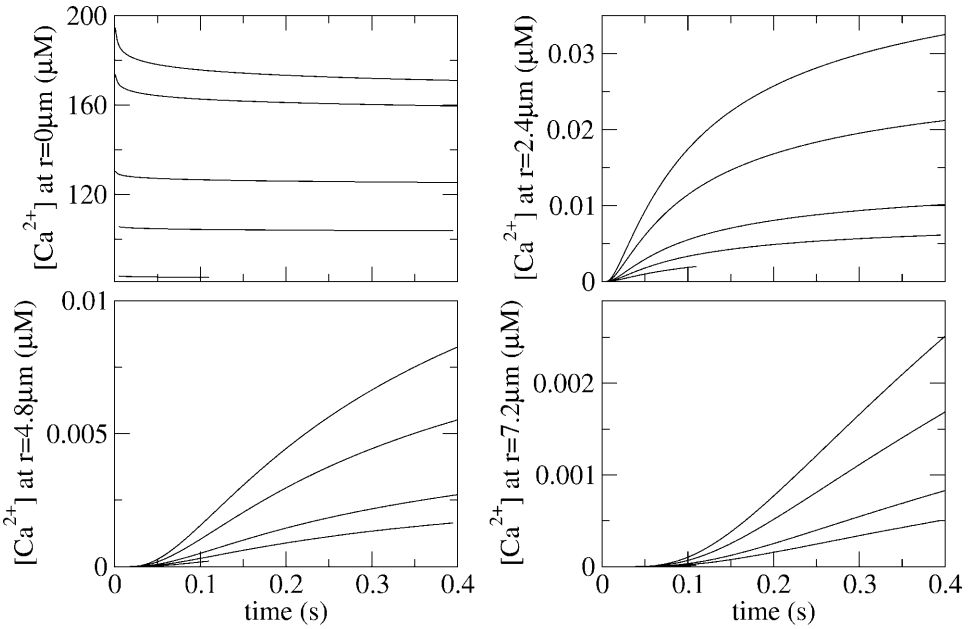

FIGURE 5 Dependence of concentration of cytosolic Ca^{2+} on time at different distances r from the channel cluster. Lines show results for 1, 2, 4, 11.11, and 21.77 open channels from lower to higher values. For parameter values, see Set 1 in Table 1. Release through a single channel was simulated for 0.115 s only.

at a distance of 2.4, 4.8, or 7.2 μm from the cluster. They grow faster with increasing current and approximately proportional to the corresponding currents.

The concentration profiles of fast mobile buffer with Ca^{2+} bound (b_m) show essentially the same behavior as the concentration of free cytosolic Ca^{2+} (Fig. 6). The buffer at the cluster saturates for $\sim$10 open channels. The concentration of free cytosolic Ca^{2+} at the cluster with a single open channel would be sufficient to saturate the buffer in a spatially homogeneous system (see Fig. 5). However, the large diffusion flux due to the large gradients prevents saturation. That is supported by a comparison with the stationary buffer, which already saturates at the cluster with a single open channel (data not shown).

Lumenal parameters

The transport properties of the lumen of the ER like diffusion coefficients or content of mobile buffer are not well known. The local concentrations of free lumenal Ca^{2+} at the cluster show that currents are determined by the transport properties

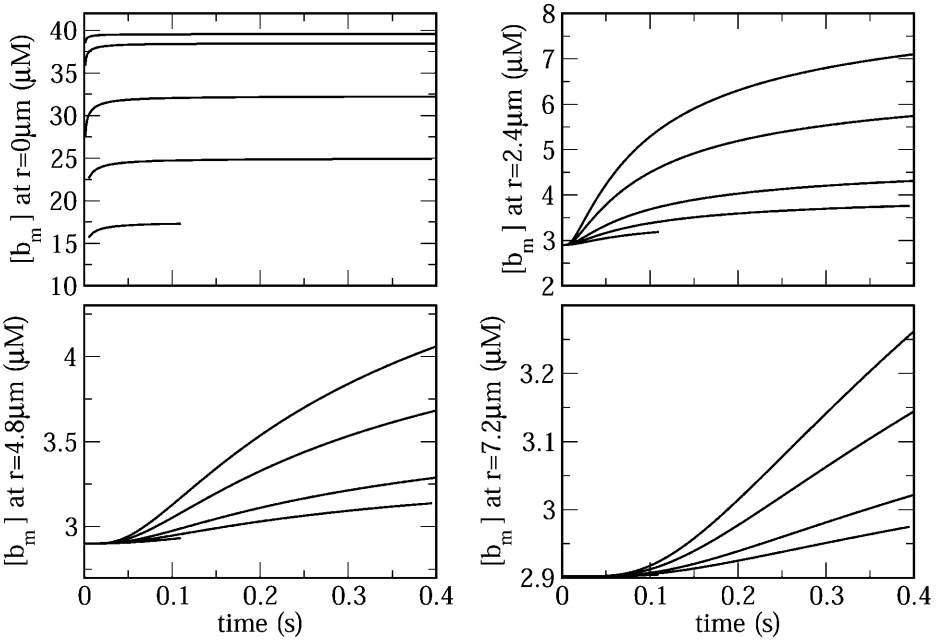

FIGURE 6 Dependence of concentration of cytosolic mobile buffer with Ca^{2+} bound on time belonging to the simulations shown in Fig. 5. The lines show results for 1, 2, 4, 11.11, and 21.77 open channels from lower to higher values. For parameter values, see Set 1 in Table 1. Release through a single channel was simulated for 0.115 s only.

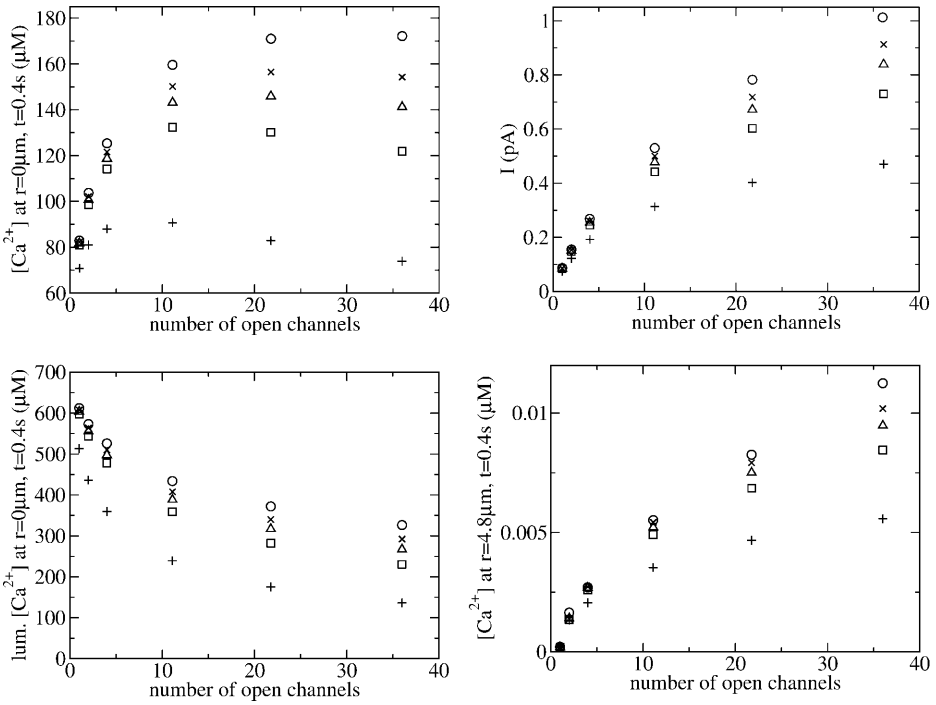

FIGURE 7 Dependence of release on the fraction of lumenal mobile buffer. (*Top left*) Concentration of free cytosolic Ca^{2+} at the cluster in dependence on the number of open channels. (*Top right*) Current values. (*Bottom left*) Concentration of free lumenal Ca^{2+} at the cluster. (*Bottom right*) Concentration of free cytosolic Ca^{2+} in a distance of 4.8 μm from the cluster. (*All panels*) Values were taken after the channels were open for 0.4 s. In case of a single open channel in the cluster, the values were obtained after 0.115 s. For parameter values, see Set 1 in Table 1 except the concentration of lumenal buffers. They are: $B_{Es} = 50$ mM, $B_{Em} = 50$ mM (○); $B_{Es} = 75$ mM, $B_{Em} = 25$ mM (X); $B_{Es} = 87.5$ mM, $B_{Em} = 12.5$ mM (△); and $B_{Es} = 100$ mM, $B_{Em} = 0$ mM (□). The values marked by (+) were obtained with $D_E = 110\ \mu m^2\ s^{-1}$ and $B_{Es} = 100$ mM, $B_{Em} = 0$mM.

because a gradient from the resting level of 715 μM far away from the cluster down to ~250 μM at the cluster builds up (Fig. 7). To understand which transport characteristics are crucial, we vary transport parameters. Changing the fraction of mobile buffer from 50% down to stationary buffer only has no major effect on currents and concentrations as Fig. 7 illustrates. Diffusion of free Ca^{2+} alone can compensate for the loss of the transport capacity of mobile buffer, if the diffusion coefficient is in the range of 223 $\mu m^2\ s^{-1}$. Reducing the diffusion coefficient of free Ca^{2+} in the ER to 110 $\mu m^2\ s^{-1}$ in the absence of mobile buffer decreases currents to a negligible degree for small numbers of open channels and by ~50% for large numbers (see Fig. 7). Because diffusion of free Ca^{2+} is crucial in determining currents, we simulated different transport conditions with the set of parameters representing an ER as a tubular meshwork as well. As mentioned above, it means reducing diffusion by one-half and setting the inner height of the ER compartment to 60 nm (see Fig. 8). Here, the larger inner height partially compensates for the smaller diffusion coefficient. Note that decreasing the diffusion coefficient again by almost a factor of 1/2 has less a relative impact than in the cisternae geometry with a lumenal height of 28 nm.

Fig. 9 shows the results for different diffusion coefficients of lumenal free Ca^{2+}. Decreasing the lumenal diffusion coefficient from the cytosolic value of 223 $\mu m^2\ s^{-1}$ down to 23 $\mu m^2\ s^{-1}$ lowers the current by about a factor of 3, but reducing it to 110 $\mu m^2\ s^{-1}$ decreases the current to ~80% of the value with the cytosolic diffusion coefficient only. Hence, if diffusion coefficients in the ER should be one-half of the cytosolic diffusion coefficients only (as discussed as a possibility above), that does not have a major impact on the release currents for not too large a number of open channels in a cluster.

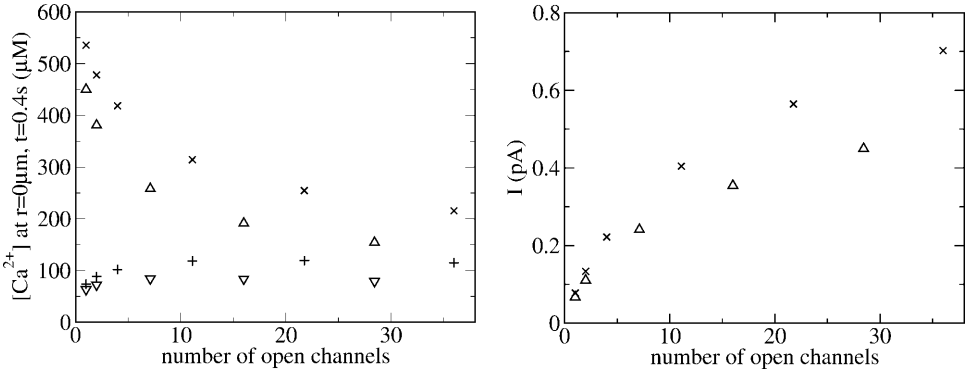

FIGURE 8 Release with parameters mimicking a tubular ER. (*Left panel*) Concentration of free Ca^{2+} at the cluster in dependence on the number of open channels. (X and +) Set 2 in Table 1, lumenal concentration (X), cytosolic concentration (+); (△ and ▽) Set 2 in Table 1 except $D_E = 63\ \mu m^2\ s^{-1}$, $D_{Em} = 8.475\ \mu m^2\ s^{-1}$, lumenal concentration (△), cytosolic concentration (▽). (*Right panel*) Currents for the same parameters as used in the simulations of the left panel. The symbols are chosen accordingly.

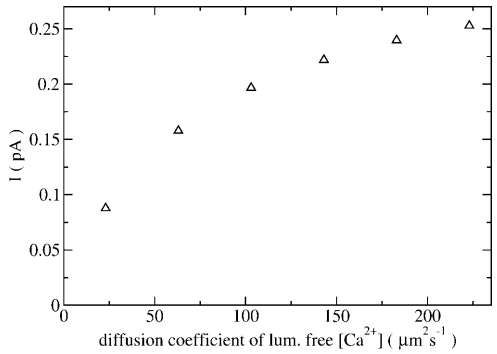

FIGURE 9 Dependence of the release current with four open channels at $t = 0.1$ s on the diffusion coefficient of lumenal free Ca^{2+} D_E. $h_{ER} = 0.028$ μm, concentration of free Ca^{2+} in the ER 715 μM, total lumenal concentration 67.87 mM, $B_{Em} = 0$, $B_{Es} = 100$ mM. For other parameter values see Set 1 of Table 1.

The major determinant of currents is the concentration of free Ca^{2+} in the ER. Fig. 10 shows results for three different concentrations of free lumenal Ca^{2+}. Note that the current through a single open channel for the lowest concentration is as small as 0.0164 pA. The cytosolic concentration of free Ca^{2+} at the location of the channel is $\sim$25 μM. Despite the nonlinear dependence of the current density on the lumenal concentration (Eq. 1), we find the current to depend linearly on the concentration of free lumenal Ca^{2+} (see Fig. 11). The linear functions approximating the curves in Fig. 11 include a constant term. Hence, the linear dependence will not hold down to $E = 0$. The approximate linearity of the currents in E arises from the almost linear dependence of the total Ca^{2+} content of the cell on E. These findings are in agreement with analytical results for a similar linearized problem in two spatial dimensions (Falcke et al., 2000b) and results by Smith (1996).

The total concentration of Ca^{2+} in the ER has little effect on the currents at least for the large radius of the ER disk and the release time of 0.4 s we are considering for the time being. Decreasing the total content from $\sim$50 mM to $\sim$5 mM changes currents at $t = 0.4$ s by $\sim$10% only. This is different for smaller radii of the lumenal compartment and longer release times as we will see below.

Cytosolic buffers, spread of released Ca^{2+} in the cytosol

In general, cytosolic concentrations of free Ca^{2+} around a cluster with open channels drop by orders of magnitude on the length of 1–2 μm already. That is illustrated by including concentration values at different distances from a cluster in Figs. 2, 5, 7, and 12. Although free Ca^{2+} reaches concentrations of several tens of micromolar at the cluster, concentration increases by a few hundred nanomolar only in a distance of $\sim$1 μm (Fig. 12) and by several nanomolar at 2.4 μm (Figs. 5 and 12).

Changing the concentration of mobile buffer in the cytosol from 40 μM to 0 μM means a change of buffer capacity B_m/K_m by $\sim$160. Currents are not influenced in a noticeable degree by such a change and neither by changing the buffer binding rates from fast to slow. Buffers could change currents by affecting the concentration of free Ca^{2+} on the cytosolic side of the cluster (see Eq. 1). However, that concentration is rather insensitive to buffer concentrations and properties. Varying buffer binding rates, buffer concentrations, buffer dissociation constants, or diffusion of mobile buffer within experimentally reasonable ranges causes changes of the concentration of free cytosolic Ca^{2+} at the cluster of $\sim$1% only.

The spread of released Ca^{2+} depends very sensitively on buffer concentrations. Hence, we can only try to determine limiting values of concentrations a few micrometers away from the cluster. We will consider the impact of concentration of fast mobile buffer, buffer binding rates for fixed dissociation constant, variation of dissociation constants of fast buffer, and buffer diffusion.

The major effect of increasing buffer binding rates is a stronger localization of the Ca^{2+} profile and larger peak values of the profile of buffer with Ca^{2+} bound. Furthermore, the rate of rise of concentrations in a fixed distance from the cluster strongly depends on buffer rates. Two observations seem remarkable here. First, the increase of diffusional spread while going from $k_m^+ = 81$ $(\mu Ms)^{-1}$ to $k_m^+ = 25$ $(\mu Ms)^{-1}$ is comparable to the effect of the much

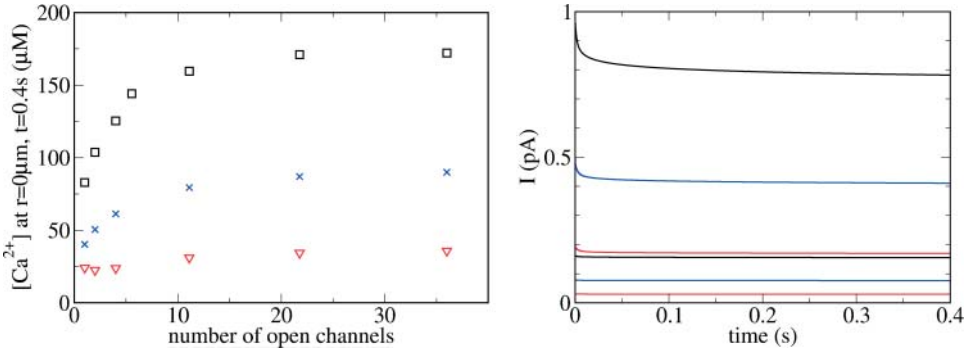

FIGURE 10 Release with different initial concentrations of free lumenal Ca^{2+}. (*Left panel*) Ca^{2+} concentration at the location of the cluster: $E = 715.56$ μM (□), total concentration of Ca^{2+} in the ER 67.87 mM; $E = 336.59$ μM (X), total concentration of Ca^{2+} in the ER 49.36 mM; and $E = 127.80$ μM (▽), total concentration of Ca^{2+} in the ER 26.87 mM. (*Right panel*) Currents for the same sets of parameters as in the right panel and for two different numbers of open channels. Matching colors have same concentration of free and total Ca^{2+} in the ER. (*For each color*) Smaller current values two open channels, larger values 21.77 open channels. Parameter values not mentioned here are those of Set 1 in Table 1.

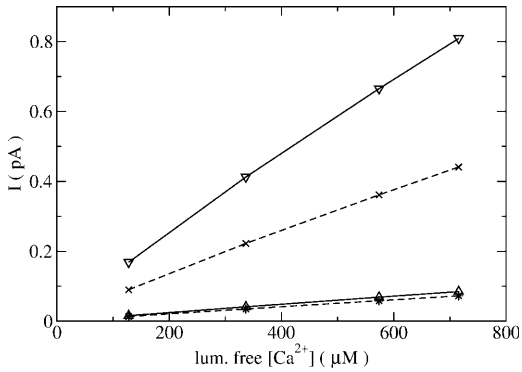

FIGURE 11 Dependence of currents at $t = 0.1$ s on the bulk concentration of free lumenal Ca^{2+}. Lumenal buffer concentrations are $B_{Es} = 100$ mM, $B_{Em} = 0$ (*solid lines*), and $B_{Es} = 10$ mM, $B_{Em} = 0$ (*dashed lines*). Small current values are obtained with one open channel and large values with 36 open channels.

larger step from $k_m^+ = 700\ (\mu Ms)^{-1}$ to $k_m^+ = 81(\mu Ms)^{-1}$. That agrees with results obtained for the stationary profiles, where major changes occurred in that range of binding constants, too (Falcke, 2003a). Hence, buffers become slow from that point of view for k^+B smaller than 800 s^{-1}. Second, facilitated diffusion of Ca^{2+} by mobile buffer is more effective with fast buffers than with slow ones. It increases the concentration compared to the case without mobile buffer beyond a certain distance from the cluster. However, that increase is in the range of a few nanomolar only.

The results for different concentrations of mobile buffer are shown in Fig. 12. Note that the increase in free Ca^{2+} concentration at $r = 4.5$ μm and $t = 0.4$ s without any mobile buffer reaches 11 nM only. Rather low concentrations of fast mobile buffer have an impact already. On length scales up to 2.5 μm, the use of 5 μM fast mobile buffer reduces the spread of free Ca^{2+} considerably. However, buffer assists spread of free Ca^{2+} by facilitated diffusion at 5 μM and 15 μM at distances larger than ~4 μm. There is essentially no difference between the results for $B_m = 30$ μM and $B_m = 40$ μM. The dissociation constant of mobile buffer has a major impact on spatial spread of free Ca^{2+} in areas, where the free Ca^{2+} concentration has approximately the value of the dissociation constant or is smaller than it. Decreasing the dissociation constant reduces the spread of free Ca^{2+}.

Varying the diffusion constant of mobile buffer D_m from 20 $\mu m^2\ s^{-1}$ to 70 $\mu m^2\ s^{-1}$ reduces the spread of free cytosolic Ca^{2+} on length scales up to 2.5 μm. The faster diffusion of mobile buffer is, the faster Ca^{2+} bound buffer can be exchanged for Ca^{2+} free buffer and the more Ca^{2+} is buffered close to the cluster. However, increasing D_m had little effect on the spread of free cytosolic Ca^{2+} to a distance of 4.5 μm. That suggests facilitated diffusion to become important on larger length scales only for large D_m.

It is often easier to measure signal mass in experiments than local rise times or concentrations. The release current can be estimated from signal mass measurements, if the fraction of Ca^{2+} binding to mobile buffer is known. The fraction of released Ca^{2+} binding to mobile buffer does essentially not depend on the current but on the buffer concentration. It increases from ~0.2 to ~0.7 when the buffer concentration is raised from 5 μM to 40 μM.

It was hypothesized by Marchant and Parker (2001) that the built-up of pacemaker Ca^{2+} has a role in wave initiation during long period wave nucleation in *Xenopus* oocytes. Pacemaker Ca^{2+} results from an incomplete decay of the concentration increase due to the previous puff at the time

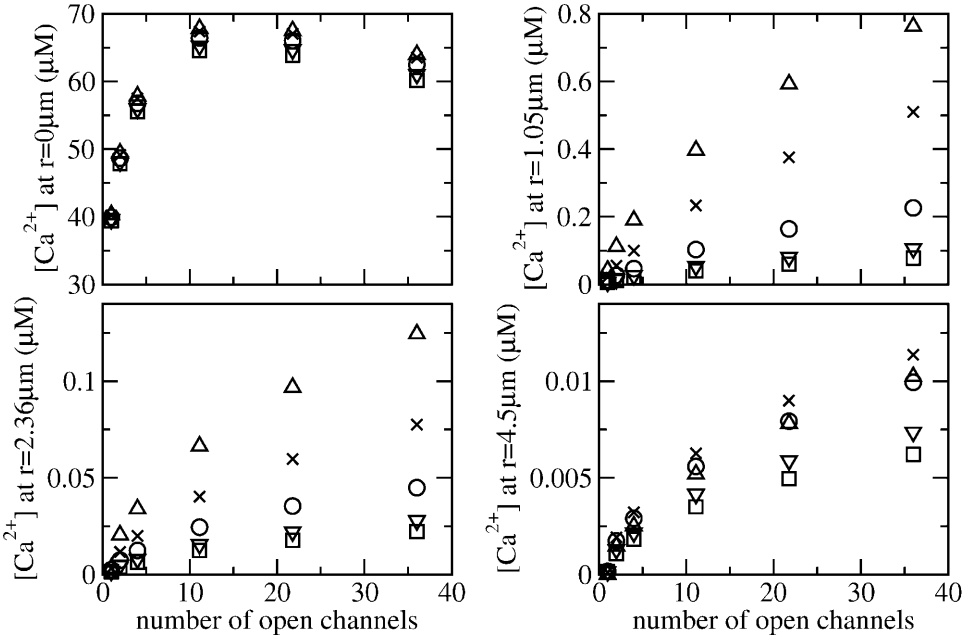

FIGURE 12 Ca^{2+} concentration at different distances from the cluster for different concentrations of mobile buffer. $B_m = 0$ μM (△), $B_m = 5$ μM (X), $B_m = 15$ μM (○), $B_m = 30$ μM (▽), $B_m = 40$ μM (□) all $k_m^+ = 700\ (\mu Ms)^{-1}$, $K_m = 0.247$ μM, and $D_m = 40$ $\mu m^2\ s^{-1}$. The currents at 0.4 s belonging to the numbers of open channels for which data are shown are: 0.041 pA (at 0.115 s), 0.071 pA, 0.119 pA, 0.218 pA, 0.299 pA, and 0.366 pA. For parameter values, see Set 1 in Table 1 except the total concentration of Ca^{2+} in the ER. It is 49 mM resulting in a resting concentration of free Ca^{2+} in the ER of 336.7 μM, $B_{Es} = 100$ mM, and $B_{Em} = 0$.

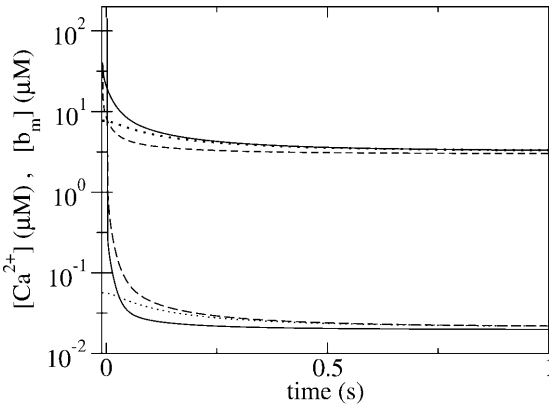

FIGURE 13 Simulation of the decay of cytosolic free Ca^{2+} c and mobile buffer with Ca^{2+} bound b_m upon termination of release after the cluster was open for 0.4 s. Note the logarithmic scale for the concentrations. Bottom group of lines c, top group of lines b_m. (*Solid lines*) Four channels open, concentration at the cluster; (*dashed lines*) 36 channels open, concentration at the cluster; and (*dotted lines*) 36 channels open, concentration 4.8 μm away from the cluster.

when another puff occurs. To obtain an estimate of the decay of cytosolic free Ca^{2+} upon closing of the last open channel in a cluster we simulated this event (see Fig. 13, Table 2). Cytosolic concentrations decay on timescales of a few tens of milliseconds at the cluster and a few hundreds of milliseconds in a distance of ~2.5 μm away from the cluster (see Table 2).

Long timescales, higher cluster density

In the previous sections we considered release for 0.4 s and a single cluster on an ER compartment with a radius of 12 μm. That setting applies to isolated puffs. Release persists for much longer times during waves or oscillations and occurs not through a single cluster but many neighbored clusters simultaneously. We can account for this by the choice of the radius of the cylinder modeling cytosol and ER shown in Fig. 1 or the radius of the lumenal compartment only. That radius determines the volume a single cluster can draw Ca^{2+} from. That volume is determined by the cluster spacing in an array of clusters. Hence, decreasing the radius of the cylinder mimics a larger density of open clusters. The distance of open clusters corresponds to twice the cylinder radius in that picture. With the radii 1 μm and 2 μm used in simulations, large currents decrease during release lasting a few seconds even with high total concentration of lumenal Ca^{2+}. At the same time, the concentration rise of free cytosolic Ca^{2+} in a distance of 4.5 μm in the direction normal to the ER surface reaches values from a few tens of nanomolar to hundreds of nanomolar.

The decay of currents within a few seconds raises the question for the timescales of this process. We simulated release for 10 s for two different ER radii and two different concentrations of total Ca^{2+} in the lumen. The experiments that can serve for comparison are superfusion experiments by Marchant and Taylor (1998). The superfusion medium is replaced every 80 ms. To be compatible with these experiments—at least as far as parameter values are known and our modeling framework allows—we set cytosolic concentration values to resting level every 80 ms and collect the amount released in 80-ms bins. The results can be fitted very well to a sum of two exponentials and a constant. The relative amplitudes of the exponentials and timescales are shown in Figs. 14 and 15. Half-times and relative amplitudes are in the range observed experimentally in hepatocytes (Marchant and Taylor, 1998; Dufour et al., 1997). The half-times decrease with increasing number of open channels, increasing cluster density, and with decreasing lumenal content. The same qualitative behavior holds for the fraction of the amplitude of the exponential with the smaller half-time. The ER with lower content can maintain release at numbers of open channels presumably typical for oscillations for ~4 s at low cluster density and ~2 s for high cluster density (estimated by twice the longer $t_{1/2}$). The ER with high content can maintain release 2–3 times longer. Hence, depletion of the ER may occur during Ca^{2+} oscillations with release phases of several seconds for low and intermediate lumenal content.

DISCUSSION

The first step of the study we have presented here is a fit of a simple single binding site expression for the channel current to data by Bezprozvanny and Ehrlich (1994). Our fit leads to a similar half-maximum value for the dependence of

TABLE 2 Timescales of the decay of free cytosolic Ca^{2+} c and mobile buffer b_m (see Fig. 13)

Species	N_O	A_0 μM	A_1 μM	λ_1 s	A_2 μM	λ_2 s	A_3 μM	λ_3 s
c	4	0.00019	0.267	0.00245	0.207	0.0125	0.0133	0.124
c	36	0.00267	1.876	0.00275	0.544	0.0144	0.0485	0.127
B_m	4	3.016	20.60	0.00210	6.386	0.0182	1.566	0.142
B_m	36	3.332	18.514	0.00346	17.787	0.0234	4.838	0.157
c, $r = 2.5$ μm	36	0.0215	0.00676	0.2049	0.00398	0.306	–	–
B_m, $r = 2.5$ μm	36	3.272	3.0204	0.0708	2.174	0.245	–	–

The decay was fit to $c(t) = A_0 + \sum_i^3 A_i e^{-t/\lambda_i}$. The fit starts 2 ms after closure of the cluster. The largest part of the profile peak is dissipated within these 2 ms. The concentrations in a distance of 2.5 μm from the cluster could be well fit to two exponentials and a constant. N_O is the number of open channels.

current on *trans* Ca^{2+} and confirms, that the feedback of *cis* Ca^{2+} on the current is negligible in the lipid bilayer experiments. However, with concentrations occurring in the ER and cytosol of a cell, this feedback becomes important. The constants obtained in this fit should apply to all IP_3R subtypes because their conduction properties are similar (Taylor, 1998). The scaling of Φ with the cross section of the single channel conducting pore has to be observed when Eq. 1 is used in other models.

We find that large gradients build up in the lumen during release, which are necessary to transport Ca^{2+} to the channel. Thus transport properties of the ER were expected to be a major factor in determining the release current. However, release currents change by ~30% only within a realistic range of diffusion coefficients of free Ca^{2+} in the ER. Neither were they very sensitive to the fraction of mobile buffer.

The proportionality of the release current to $N_O^{1/m}$ with $m \geq 2$ is important for interpreting experiments of the IP_3 dependence of release currents. As an example we consider results by Parker et al. (1996b) on the increase of the initial release rate with IP_3 in local measurements. The initial rate raises like 120 $(\mu Ms)^{-1}$ $[IP_3]/([IP_3] + 600$ nM). If we assume that IP_3 needs to bind in a noncooperative way to two subunits for the channel to open, the number of open channels N_O is proportional to $([IP_3]/([IP_3]+K_{IP_3}))^2$ and hence the current to $[IP_3]/([IP_3]+K_{IP_3})$. Note that our results cannot be directly transferred to global measurements because global release might increase by opening of channels situated not close to an open channel.

Currents in our simulations are in the range from 0.015 pA ($E = 127$ μM, one open channel) to 0.8 pA ($E = 715$ μM, 36 open channels). We can compare this to signal mass released in *Xenopus* oocytes, because signal mass was found to be the most reliable measurement in characterization of puffs (Sun et al., 1998). According to Sun et al. (1998), between 0.004 pC and 0.22 pC are released during puffs (most of them release <0.12 pC). The amount of Ca^{2+} released in 0.4 s in our simulations spans the range from 0.006 pC to 0.32 pC. Hence, it covers the range measured in *Xenopus* oocytes. We can compare more specifically the signal mass for five open channels and different values of free lumenal concentrations. The number of five open channels is typical for a puff (Sun et al., 1998). That is 0.021 pC at $E = 127$ μM and 0.055 pC at $E = 336$ μM. Sun et al. assume that one-half of the released Ca^{2+} binds to the dye. However, we find that 70% bind to the dye at a dye concentration of 40 μM. Hence, most of the puffs reported in Sun et al. (1998) are actually below 0.0857 pC. If we further assume puffs with a large signal mass to last 600 ms instead of 400 ms (see Sun et al., 1998), we need to multiply the simulated values with a factor 1.5. Finally, we find that the range of signal mass in our simulations agrees with the range found for puffs in *Xenopus* oocytes, if the concentration of free lumenal Ca^{2+} is between 127 μM and 336 μM. That is in agreement with recent measurements of free lumenal Ca^{2+} in *Xenopus* oocytes (Falcke et al., 2003).

The increase of cytosolic Ca^{2+} in a distance of 4.5 μm from an open channel after 0.4 s of release is rather small. It stays below 15 nM in the examples we have presented. If the resting concentration is 100 nM (40 nM) and three Ca^{2+} ions need to bind for the channel to open, then a rise of 15 nM increases the opening probability per unit time by a factor of 1.52 (2.6). According to recent measurements, a resting level of 100 nM appears more realistic in *Xenopus* oocyte (Falcke et al., 2003). The rather small increase in the open probability caused by releasing clusters in the vicinity of a closed cluster coincides with the finding that a single puff cannot initiate a wave (Marchant and Parker, 2001). If there are three releasing clusters in the vicinity of a closed cluster, the open probability already increases by a factor of 3.05 (resting level 100 nM).

The timescale of the decay of concentration profiles upon the termination of release can be set in relation to puff frequencies just below the wave initiation threshold (Marchant et al., 1999). Marchant et al. measured the distribution of time intervals between puffs. The distribution has a peak for 1.5–2 s and falls to half the peak value in the bin 0–0.5 s (Marchant et al., 1999). Hence, an impact of local pacemaker Ca^{2+} on puff behavior would require that the IP_3Rs are able to sense concentration differences in the nM range and that the puff frequency is ~3 s^{-1}. These considerations apply, if diffusion dissipates release profiles completely. Pacemaker Ca^{2+} can of course still occur as global concentration increase in which case its dynamics is determined by other processes than diffusion.

Buffers had essentially no effect on the peak concentration values of free cytosolic Ca^{2+} at the channel cluster in our simulations. This is important in assessing experiments using buffers to eliminate feedback of Ca^{2+} on the channel dynamics. Typically, high concentrations of EGTA are used. The full width at half-maximum is 10.7 nm only with 2 mM buffer concentration in our simulations. However, the half-maximum is still a concentration of a few tens of micromolar of free Ca^{2+} typically, which is capable of exerting a feedback on channel behavior.

Most simplified models up to date couple regulation of the channel to the average bulk concentration. However, the concentration experienced by the regulatory binding sites of the IP_3R is 2–3 orders of magnitude larger than the average bulk concentration. Most models of channel dynamics assume dissociation constants for binding of Ca^{2+} to the activating binding site in the submicromolar range. Furthermore, lipid bilayer experiments using cations different from Ca^{2+} as the ion conducted by the IP_3R—hence allowing for separate control of the Ca^{2+} concentration on the *cis* side—indicate that these dissociation constants are realistic indeed (Ramos-Franco et al., 1998; Mak et al., 1998, 1999, 2001). Additionally, if channels are able to sense an open cluster 2–5 μm away or pacemaker Ca^{2+}, they need to be

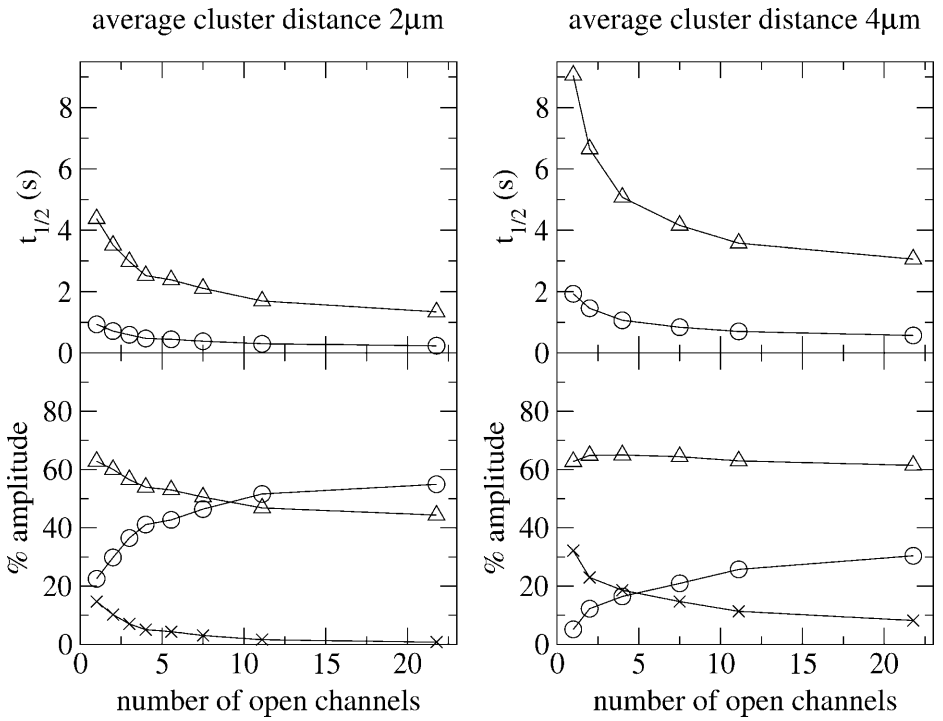

FIGURE 14 Analysis of the temporal decay of release from the ER with high initial lumenal content. Amounts released within 80 ms were sampled in bins. The result was fitted to $A_0+A_1 e^{(t\ln 2)/t^1_{1/2}}+A_2 e^{(t\ln 2)/t^2_{1/2}}$. The symbols of the amplitude curves match the symbols of the corresponding $t_{1/2}$. X marks the contribution of the constant term. (*Left*) Radius of the lumenal compartment is 1 μm corresponding to an average cluster distance of 2 μm. (*Right*) Radius of the lumenal compartment is 2 μm corresponding to an average cluster distance of 4 μm. The upper row shows the $t_{1/2}$, the lower row the relative amplitude. Initial concentration of free lumenal Ca^{2+} $E = 715.56$ μM, initial total concentration of Ca^{2+} in the ER 67.87 mM, $P_p = P_l = 0$.

able to sense concentration changes in the nanomolar range. These findings and considerations entail a very high opening probability for all IP_3-bound channels of a cluster as soon as the first channel of a cluster opens, because the dissociation constant of the activating Ca^{2+} binding site is much smaller than the concentrations at the cluster location. Together with the large spatial gradients occurring around an open cluster, that will have consequences for the existence and stability of asymptotic solutions of deterministic cluster models. We will discuss that topic in an upcoming report.

The timescales and the amplitudes of the exponential functions describing the decay of currents in simulations over 10 s (Figs. 14 and 15) are in the range of but not equal to experimentally determined values (Marchant and Taylor,

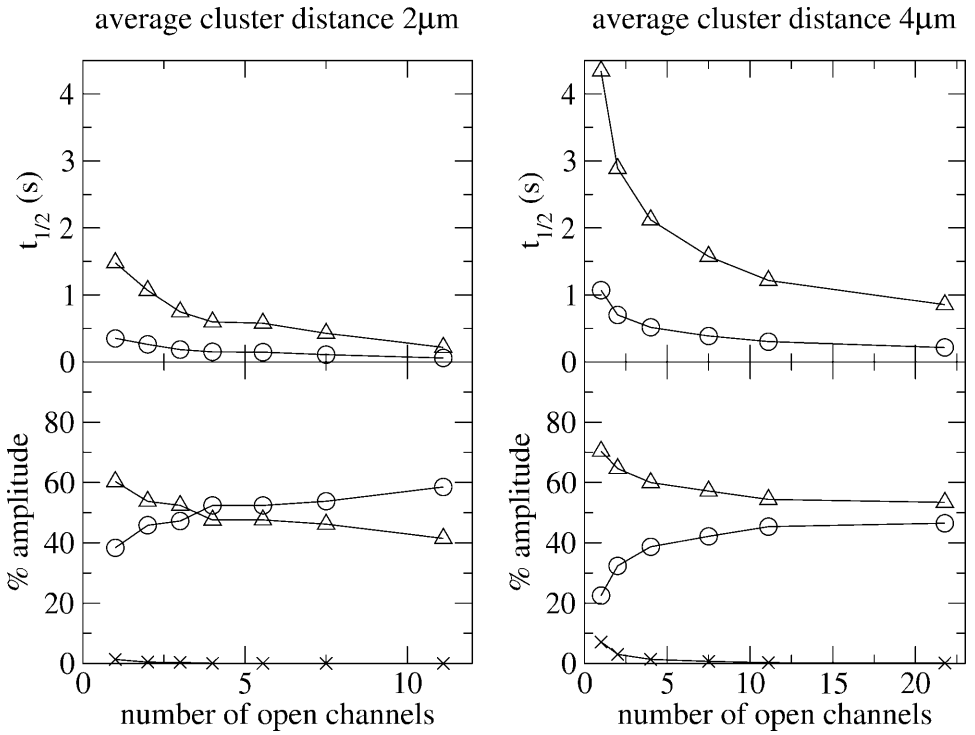

FIGURE 15 Analysis of the temporal decay of release from the ER with low initial lumenal content. Amounts released within 80 ms were sampled in bins. The result was fitted to $A_0+A_1 e^{(t\ln 2)/t^1_{1/2}}+A_2 e^{(t\ln 2)/t^2_{1/2}}$. The symbols of the amplitude curves match the symbols of the corresponding $t_{1/2}$. X marks the contribution of the constant term. (*Left*) Radius of the lumenal compartment is 1 μm corresponding to an average cluster distance of 2 μm. (*Right*) Radius of the lumenal compartment is 2 μm corresponding to an average cluster distance of 4 μm. The upper row shows the $t_{1/2}$, the lower row the relative amplitude. Initial concentration of free lumenal Ca^{2+} $E = 336.6$ μM, initial total concentration of Ca^{2+} in the ER 5.24 mM, $P_p = P_l = 0$.

1998; Dufour et al., 1997). These values are obtained in experiments designed to evaluate timescales of channel dynamics. The smallest $t_{1/2}$ we find are larger than the experimental values when a high lumenal content is used in the simulation but smaller when we apply a low lumenal content (Marchant and Taylor, 1998). An analysis based on better knowledge of lumenal parameters would be necessary to assess the meaning of these findings for experimental results. However, conclusions on channel state dynamics cannot be drawn from the mere existence of more than one timescale in current decay.

The geometry we have chosen for our simulations applies best to cisternae of the ER because it allows for diffusion into half-space only. The radius of tubes is assumed to be 30 nm (Alberts et al., 1994). The gradient of profiles created by small currents (<0.1 pA) decreases by ~80% on this length scale and clusters creating this current have a radius much smaller than the tube radius. Hence, for small clusters, the tube will essentially act like the membrane of a cisternae. The Ca^{2+} gradient created by currents in the range of 0.3 pA decreases by ~50% on the first 30 nm. Hence, diffusion "around" the tube will have an impact. However, the reduced peak value of cytosolic Ca^{2+} due to diffusion increases the difference $E - \alpha c$ in Eq. 1, which increases the current and hence counteracts the decrease of cytosolic Ca^{2+}. Therefore, we assume that our simulations are a good approximation for Ca^{2+} concentration profiles close to a cluster on a tube of the ER as well. The results, which will depend on whether cisternae or tubular ER is modeled, are the timescales of the decay of currents.

In summary, our results provide information on the relation of currents to the number of open channels and current values to the concentration of free lumenal Ca^{2+}, which assist in the analysis of experimental results. We provide ranges of values for concentrations and concentration gradients on which modeling can be based.

REFERENCES

Alberts, B., D. Bray, J. Lewis, M. Raff, K. Roberts, and J. Watson. 1994. Molecular Biology of the Cell, 3rd ed. Garland Publishing, Inc., New York, NY and London, UK.

Allbritton, N., T. Meyer, and L. Sryer. 1992. Range of messenger action of calcium ion and inositol 1,4,5 trisphosphate. *Science*. 258:1812–1815.

Atri, A., J. Amundson, D. Clapham, and J. Sneyd. 1993. A single pool model for intracellular calcium oscillations and waves in the Xenopus laevis oocyte. *Biophys. J.* 65:1727–1739.

Bär, M., M. Falcke, L. Tsimring, and H. Levine. 2000. Discrete stochastic modeling of calcium channel dynamics. *Phys. Rev. Lett.* 84:5664–5667.

Berridge, M. 1993. Inositol trisphosphate and calcium signalling. *Nature*. 361:315–325.

Berridge, M. 1997. Elementary and global aspects of calcium signalling. *J. Physiol.* 499:291–306.

Berridge, M., M. Bootman, and P. Lipp. 1998. Calcium: a life and death signal. *Nature*. 395:645–648.

Bezprozvanny, I., and B. Ehrlich. 1994. Inositol(1,4,5)-trisphosphate Ins(1,4,5)P_3-gated channels from cerebellum: conduction properties for divalent cations and regulation by intraluminal calcium. *J. Gen. Physiol.* 104:821–856.

Blatter, L., J. Hüser, and E. Rios. 1997. Sarcopasmic reticulum Ca^{2+} release flux underlying Ca^{2+} sparks in cardiac muscle. *Proc. Natl. Acad. Sci. USA*. 94:4176–4181.

Bootman, M., M. Berridge, and P. Lipp. 1997. Cooking with calcium: the recipes for composing global signals from elementary events. *Cell*. 91:367–373.

Bootman, M., T. Collins, C. Peppiatt, L. Prothero, L. MacKenzie, P. DeSmet, M. Travers, S. Tovey, J. Seo, M. Berridge, F. Ciccolini, and P. Lipp. 2001. Calcium signalling: an overview. *Semin. Cell Dev. Biol.* 12:3–10.

Borghans, J., G. Dupont, and A. Goldbeter. 1997. Complex intracellular calcium oscillations: a theoretical exploration of possible mechanisms. *Biophys. Chem.* 66:25–41.

Camacho, P., and J. Lechleiter. 1995. Calreticulin inhibits repetitive intracellular Ca^{2+} waves. *Cell*. 82:756–771.

Coombes, S. 2001. The effect of ion pumps on the speed of travelling waves in the fire-diffuse-fire model of Ca^{2+} release. *Bull. Math. Biol.* 63:1–20.

D'Andrea, P., and F. Vittur. 1995. Spatial and temporal Ca^{2+} signalling in articular chondrocytes. *Biochem. Biophys. Res. Commun.* 75:129–135.

DeYoung, G., and J. Keizer. 1992. A single-pool inositol 1,4,5-trisphosphate-receptor-based model for agonist-stimulated oscillations in Ca^{2+} concentration. *Proc. Natl. Acad. Sci. USA*. 89:9895–9899.

Dufour, J., I. Arias, and T. Turner. 1997. Inositol 1,4,5-trisphosphate and calcium regulate the calcium channel function of the hepatic inositol 1,4,5-trisphosphate receptor. *J. Biol. Chem.* 272:2675–2681.

Dupont, G., and A. Goldbeter. 1993. One-pool model for Ca^{2+} oscillations involving Ca^{2+} and inositol 1,4,5-trisphosphate as co-agonists for Ca^{2+} release. *Cell Calcium*. 14:311–322.

Dupont, G., and A. Goldbeter. 1994. Properties of intracellular Ca^{2+} waves generated by a model based on Ca^{2+}-induced Ca^{2+} release. *Biophys. J.* 67:2191–2204.

Falcke, M. 2003a. Buffers and oscillations in intracellular Ca^{2+} dynamics. *Biophys. J.* 84:28–41.

Falcke, M. 2003b. On the role of stochastic channel behavior in intracellular Ca^{2+} dynamics. *Biophys. J.* 84:42–56.

Falcke, M., M. Bär, J. Lechleiter, and J. Hudson. 1999a. Spiral breakup and defect dynamics in a model for intracellular Ca^{2+} dynamics. *Physica D*. 129:236–252.

Falcke, M., J. Hudson, P. Camacho, and J. Lechleiter. 1999b. Impact of mitochondrial Ca^{2+} cycling on pattern formation and stability. *Biophys. J.* 77:37–44.

Falcke, M., Y. Li, J. Lechleiter, and P. Camacho. 2003. Modeling the dependence of the period of intracellular Ca^{2+} waves on SERCA expression. *Biophys. J.* 85:1474–1481.

Falcke, M., M. Or-Guil, and M. Bär. 2000a. Dispersion gap and localized spiral waves in a model for intracellular Ca^{2+} dynamics. *Phys. Rev. Lett.* 84:4753–4756.

Falcke, M., L. Tsimring, and H. Levine. 2000b. Stochastic spreading of intracellular Ca^{2+} release. *Phys. Rev. E*. 62:2636–2643.

Foyouzi-Youssefi, R., S. Arnaudeau, C. Borner, W. Kelley, J. Tschopp, D. Lew, N. Demaurex, and K.-H. Krause. 2000. Bcl-2 decreases the free Ca^{2+} concentration within the endoplasmic reticulum. *Proc. Natl. Acad. Sci. USA*. 97:5723–5728.

Gonzalez, A., W. Kirsch, N. Shirokova, G. Pizarro, I. Pessah, M. Stern, H. Cheng, and E. Rios. 2000. Involvement of multiple intracellular release channels in calcium sparks of skeletal muscle. *Proc. Natl. Acad. Sci. USA*. 97:4380–4385.

Hille, B. 2001. Ion Channels of Excitable Membranes, 3rd ed. Sinauer Assoicates, Inc. Publishers, Sunderland, MA.

Hofer, A., and I. Schulz. 1996. Quantification of intraluminal free [Ca^{2+}] in the agonist-sensitive internal calcium store using compartmentalized fluorescent indicatos: some considerations. *Cell Calcium*. 20:235–242.

Izu, L., J. Mauban, C. Balke, and W. Wier. 2001. Large currents generate cardiac Ca^{2+} sparks. *Biophys. J.* 80:88–102.

John, L., J. Lechleiter, and P. Camacho. 1998. Differential modulation of SERCA2 isoforms by calreticulin. *J. Cell Biol.* 142:963–973.

Keener, J., and J. Sneyd. 1998. Mathematical Physiology. Springer, New York.

Kushmerick, M., and R. Podolsky. 1969. Ion mobility in muscle cells. *Science.* 166:1287–1298.

Lechleiter, J., S. Girard, D. Clapham, and E. Peralta. 1991. Subcellular patterns of calcium release determined by g-protein-specific residues of muscarinic receptors. *Nature.* 350:505–508.

Lindsay, A., and A. Williams. 1991. Functional characterization of the ryanodine receptor purified from sheep cardiac muscle sarcoplasmic reticulum. *Biochim. Biophys. Acta.* 1064:89–102.

Lindsay, A., S. Manning, and A. Williams. 1991. Monovalent cation conductance in the ryanodine receptor-channel of sheep cardiac muscle sarcoplasmic reticulum. *J. Physiol.* 439:463–480.

Mak, D., and J. Foskett. 1997. Single-channel kinetics, inactivation, and spatial distribution of inositol trisphophate (IP_3) receptor in Xenopus oocyte nucleus. *J. Gen. Physiol.* 109:571–587.

Mak, D., and J. Foskett. 1998. Effects of divalent cations on single-channel conduction properties of Xenopus IP_3 receptor. *Am. J. Physiol.* 275:C179–C188.

Mak, D., S. McBride, and J. Foskett. 1998. Inositol 1,4,5-tris-phosphate activation of inositol tris-phosphate receptor Ca^{2+} channel by ligand tuning of Ca^{2+} inhibition. *Proc. Natl. Acad. Sci. USA.* 95:15821–15825.

Mak, D., S. McBride, and J. Foskett. 1999. ATP regulation of type 1 inositol 1,4,5-trisphosphate receptor channel gating by allosteric tuning of Ca^{2+} activation. *J. Biol. Chem.* 274:22231–22237.

Mak, D., S. McBride, and J. Foskett. 2001. Regulation by Ca^{2+} and inositol 1,4,5-trisphosphate ($InsP_3$) of single recombinant type 3 $InsP_3$ receptor channels: activation uniquely distinguishes type 1 and type 3 $InsP_3$ receptors. *J. Gen. Physiol.* 117:435–446.

Mak, D., S. McBride, V. Raghuram, Y. Yue, S. Joseph, and J. Foskett. 2000. Single-channel properties in endoplasmic reticulum membrane of recombinant type 3 inositol trisphosphate receptor. *J. Gen. Physiol.* 115:241–255.

Marchant, J., and I. Parker. 2001. Role of elementary Ca^{2+} puffs in generating repetitive Ca^{2+} oscillations. *EMBO J.* 20:65–76.

Marchant, J., and C. Taylor. 1998. Rapid activation and partial inactivation of inositol trisphosphate receptors by inositol trisphosphate. *Biochemistry.* 37:11524–11533.

Marchant, J., N. Callamaras, and I. Parker. 1999. Initiation of IP_3-mediated Ca^{2+} waves in Xenopus oocytes. *EMBO J.* 18:5285–5299.

Mejia-Alvarez, R., C. Kettlun, E. Rios, and M. Stern. 1999. Unitary calcium current through cardiac ryanodine receptors under physiological conditions. *J. Gen. Physiol.* 113:177–186.

Meldolesi, J., and T. Pozzan. 1998. The endoplasmic reticulum Ca^{2+} store: a view from the lumen. *Trends Biochem. Sci.* 23:10–14.

Melzer, W., E. Rios, and M. Schneider. 1984. Time course of calcium release and removal in skeletal muscle fibers. *Biophys. J.* 45:637–641.

Melzer, W., E. Rios, and M. Schneider. 1987. A general procedure for determining the rate of calcium release from the sarcoplasmic reticulum in skeletal muscle fibers. *Biophys. J.* 51:849–863.

Michalak, M., R. Milner, K. Burns, and M. Opas. 1992. Calreticulin. *Biochem. J.* 285:681–692.

Miyawaki, A., J. Llopis, R. Heim, J. McCaffery, J. Adams, M. Ikura, and R. Tsien. 1997. Fluorescent indicators for Ca^{2+} based on green fluorescent proteins and calmodulin. *Nature.* 388:882–887.

Nathanson, H., A. Burgstahler, and M. Fallon. 1994. Multistep mechanism of polarized Ca^{2+} wave patterns in hepatocytes. *Am. J. Physiol.* 267:G338–G349.

Ölveczky, B., and A. Verkman. 1998. Monte carlo analysis of obstructed diffusion in three dimensions: application to molecular diffusion in organelles. *Biophys. J.* 74:2722–2730.

Parker, I., J. Choi, and Y. Yao. 1996a. Elementary events of $InsP_3$-induced Ca^{2+} liberation in Xenopus oocytes: hot spots, puffs and blips. *Cell Calcium.* 20:105–121.

Parker, I., Y. Yao, and V. Ilyin. 1996b. Fast kinetics of calcium liberation induced in Xenopus oocytes by photoreleased inositol trisphosphate. *Biophys. J.* 70:222–237.

Pratusevitch, V., and C. Balke. 1996. Factors shaping the confocal image of calcium spark in cardiac muscle cells. *Biophys. J.* 71:2942–2957.

Press, W., S. Teukolsky, W. Vetterling, and B. Flannery. 1992. Numerical Recipes in C, 2nd ed. Cambridge University Press, Cambridge, UK.

Ramos-Franco, J., M. Fill, and G. Mignery. 1998. Isoform-specific function of single inositol 1,4,5-trisphosphate receptor channels. *Biophys. J.* 75: 834–839.

Ridgway, E., J. Gilkey, and L. Jaffe. 1977. Free calcium increases explosively in activating medaka eggs. *Proc. Natl. Acad. Sci. USA.* 74:623–627.

Rios, E., M. Stern, A. Gonzalez, and G. Pizarro. 1999. Calcium release flux underlying Ca^{2+} sparks of frog skeletal muscle. *J. Gen. Physiol.* 114:31–48.

Robert, V., F. DeGiorgi, M. Massimino, M. Cantini, and T. Pozzan. 1998. Direct monitoring of the calcium concentration in the sarcoplasmic and endoplasmic reticulum of skeletal muscle myotubes. *J. Biol. Chem.* 273:30372–30378.

Roderick, H., D. Llewellyn, A. Campbell, and J. Kendall. 1998. Role of calreticulin in regulating intracellular Ca^{2+} storage and capacitative Ca^{2+} entry in hela cells. *Cell Calcium.* 24:253–262.

Smith, G. 1996. Analytical steady-state solution to the rapid buffer approximation near an open Ca^{2+} channel. *Biophys. J.* 71:3064–3072.

Smith, G., L. Dai, R. Miura, and A. Sherman. 2001. Asymptotic analysis of buffered calcium diffusion near a point source. *SIAM J. Appl. Math.* 61:1816–1838.

Smith, G., J. Keizer, M. Stern, W. Lederer, and H. Cheng. 1998. A simple numerical model of calcium spark formation and detection in cardiac myocytes. *Biophys. J.* 75:15–32.

Sneyd, J., and J.-F. Dufour. 2002. A dynamic model of the type-2 inositol trisphosphate receptor. *Proc. Natl. Acad. Sci. USA.* 99:2398–2403.

Sneyd, J., and J. Sherrat. 1997. On the propagation of calcium waves in an inhomogeneous medium. *SIAM J. Appl. Math.* 57:73–94.

Sneyd, J., S. Girard, and D. Clapham. 1993. Calcium wave propagation by calcium induced calcium release: an unusual excitable system. *Bull. Math. Biol.* 55:315–344.

Sun, X.-P., N. Callamaras, J. Marchant, and I. Parker. 1998. A continuum of $InsP_3$-mediated elementary Ca^{2+} signalling events in Xenopus oocytes. *J. Physiol. (Lond.).* 509:67–80.

Swillens, S., P. Champeil, L. Combettes, and G. Dupont. 1998. Stochastic simulation of a single inositol 1,4,5-trisphoasphate-sensitive Ca^{2+} channel reveals repetitive openings during blip-like Ca^{2+} transients. *Cell Calcium.* 23:291–302.

Swillens, S., G. Dupont, and P. Champeil. 1999. From calcium blips to calcium puffs: theoretical analysis of the requirements for interchannel communication. *Proc. Natl. Acad. Sci. USA.* 96:13750–13755.

Taylor, C. 1998. Inositol trisphosphate receptors: Ca^{2+}-modulatd intracellular Ca^{2+} channels. *Biochim. Biophys. Acta.* 1436:19–33.

Thomas, D., P. Lipp, M. Berridge, and M. Bootman. 1998. Hormone-evoked elementary Ca^{2+} signals are not stereotypic, but reflect activation of different size channel clusters and variable recruitment of channels within a cluster. *J. Biol. Chem.* 273:27130–27136.

Wagner, J., and J. Keizer. 1994. Effects of rapid buffers on Ca^{2+} oscillations and Ca^{2+} diffusion. *Biophys. J.* 67:447–456.

Wang, S.-H., and S. Thompson. 1995. Local positive feedback by calcium in the propagation of intracellular calcium waves. *Biophys. J.* 69:1683–1697.

Wilson, B., J. Pfeiffer, A. Smith, J. Oliver, J. Oberdorf, and R. Wojcikiewicz. 1998. Calcium-dependent clustering of inositol 1,4,5-trisphosphate receptors. *Mol. Biol. Cell.* 9:1465–1478.

Zhou, Z., and E. Neher. 1993. Mobile and immobile calcium buffers in bovine adrenal chromaffin cells. *J. Physiol.* 469:245–273.